

Thermodynamics of low-dimensional adsorption in grooves, on the outer surface, and in interstitials of a closed-ended carbon nanotube bundle

T. N. Antsygina, I. I. Poltavsky, and K. A. Chishko*

B. Verkin Institute for Low Temperature Physics and Engineering, 47 Lenin Avenue, 61103 Kharkov, Ukraine

(Received 7 September 2006; revised manuscript received 17 October 2006; published 22 November 2006)

The thermodynamics of an atomic deposit adsorbed in grooves, on the outer surface, and in interstitials of a closed-end carbon nanobundle is investigated theoretically. The model takes into account the interparticle interaction in the primary and secondary chains of the groove subsystem as well as the interaction between atoms from different chains. The thermodynamic potential for the groove subsystem is calculated exactly within the transfer-matrix method. The interstitials, two-dimensional deposit on the outer bundle surface and three-dimensional atmosphere of the cell, are included into consideration through the appropriate balance condition. The average adsorbate densities, adsorption isotherms, isosteric heat, and heat capacity are calculated. The behavior of these quantities is analyzed in detail at different relations between the parameters of the system. The theoretical results are in good quantitative agreement with the experimental data on thermodynamics of ^4He adsorbate.

DOI: [10.1103/PhysRevB.74.205429](https://doi.org/10.1103/PhysRevB.74.205429)

PACS number(s): 61.46.Fg, 68.43.De, 68.43.Fg

I. INTRODUCTION

Theoretical and experimental study of multilayer adsorption is of great interest due to an intensive development of nanotechnology. To construct devices with specified characteristics we need tools to operate on electrical, mechanical, and structure properties of nanotubes and nanobundles. The dosing adsorption of atomic and molecular deposits is one of such tools. That is why a comprehensive investigation of physical processes responsible for adsorption on nanobundles is of great importance to the modern nanoscience.^{1–8}

At present various aspects of atomic and molecular adsorption on planar graphite and metallic substrates are well understood.^{9–17} A carbon nanobundle, as a substrate, differs substantially from the planar graphite. First, the bundle has positions where the one-dimensional (1D) deposit can be formed. They are intratube channels if the bundle consists of open nanotubes, interstitials, and also grooves on the outer surface of the bundle. All these positions are different not only in binding energies between a particle and the substrate but also in conditions for deposition of adsorbate particles. Namely, interstitials are accessible for deposition if their cross sizes exceed the diameter of an adsorbate particle. Inside a nanotube the particles may occupy either positions on the intrinsic wall of the tube or axial positions along the tube, depending on the relation between the diameters of an intratube channel and adsorbate atom. At depositing on the outer surface the particles first occupy the bottom of the groove forming a primary chain, and then with increasing in coverage two secondary chains appear and the 1D condensate changes to a three-chain groove structure (GS). At large coverages the two-dimensional (2D) adsorbate develops on the outer surface of nanobundles. Due to substantial curvature of the bundle surface the 2D positions on it differ considerably from those on the planar graphite. The numbers of possible 1D and 2D positions on the bundle surface are comparable in magnitude.

Until the present time the thermodynamics of adsorbates on nanobundles was studied for the most part by numerical

methods, in particular, by Monte Carlo (MC) simulation. Within this approach the main attention was paid to the adsorption potentials,^{18,19} binding energy, and corrugation effects which influence the adsorbate formation in the external grooves^{20–23} and outer surface of the bundle. The potentials and binding energy for adsorption into interstitials were also discussed.^{19,23–26} As for thermodynamic functions of the low-dimensional adsorbate, the intrinsic energies of helium,²⁶ hydrogen,¹⁹ the heat capacities of helium,²⁷ argon,²⁸ and isosteric heat of methane²⁹ were calculated using various MC algorithms. Numerical simulations such as MC are believed to give the most direct way to describe complicated statistical systems, but in reality the accuracy of MC results is limited for some reasons. First, the modeling procedures operate only with small amounts of particles (typically, not more than 40–60 particles²⁸), so that the extension of the results on the real many-body system needs special justification. Second, all the parameters of the system should be specified numerically for each run of the procedure and for the new set of the parameters the procedure should be repeated again, which makes it difficult to find in details how the result depends on the parameters of the system.

In this connection various analytical methods are of great importance to treat the thermodynamics of adsorption on nanobundles. In Ref. 30 the quantum virial expansion was employed to calculate the specific heat of the 1D adsorbate with regard to the interparticle interaction. In Ref. 31 the one-particle energy-band structure of He atom in a corrugated interstitial channel was analyzed and the contribution from the interstitials to the adsorbate heat capacity was estimated. In Ref. 32 analytical expressions for the phonon excitation spectrum of the 1D dense deposit in bundle external grooves were obtained and the specific heat of this linear phase was calculated.

Recently, an analytical approach³³ based on a lattice gas model has been proposed to describe the thermodynamics of particles adsorbed in the grooves of carbon nanobundles. Despite the set of simplifications the model³³ is adequate for interpreting the adsorption on the initial stage of deposition

(groove phase formation). The results obtained in Ref. 33 are in good agreement with the experimental data^{1,2,33} on thermodynamic properties of helium and methane adsorbates.

In the present paper we improve the approach³³ by taking into account the interparticle interaction between nearest (NN) and next nearest (NNN) neighbors in the three-chain groove phase and by including interstitials and the 2D subsystem into consideration. As is shown below, the main part of the problem relating to the three-chain subsystem reduces to the exact-solvable model of the statistical physics, and rigorous analytical results can be obtained at arbitrary values of interparticle interaction parameters.

The plan of the paper is as follows. In Sec. II, we introduce and justify the Hamiltonian for the quasi-1D multilayer adsorbate (three-chain groove structure). In Sec. III, the transfer-matrix and grand canonical partition function for the GS are built and the conservation law for the total number of the particles in the system is derived. In Sec. IV, we calculate the thermodynamic functions of the adsorbate (adsorbate density, isosteric heat, and heat capacity) and analyze their behavior at various relations between the interparticle interaction parameters. The role of interstitials in the low-dimensional adsorption is discussed in Sec. V. In Sec. VI, on the basis of the present theory we give the quantitative interpretation of the experimental data on the adsorption isotherms and isosteric heat.

II. STATEMENT OF THE PROBLEM

Let us assume that a monoatomic gas is adsorbed on a nanobundle made of closed nanotubes. Then, the intratube adsorption is not possible. The system of N particles consists of a low-dimensional subsystem (adsorbate) with the average density n_{ads} , and a three-dimensional (3D) atmosphere with the density n_{3D} . The 3D subsystem is considered as an ideal lattice gas³⁴ with the internal energy $\varepsilon_{3D}=0$. Thus, the 3D atmosphere is simply the reservoir of the particles whose balance with the other parts of the system is determined by the thermodynamic equilibrium conditions.³⁴

The low-dimensional subsystem includes 2D positions on the curved outer bundle surface and a quasi-one-dimensional subsystem that consists of the three-chain structure formed in grooves and deposits in the interstitials (Fig. 1). The basic part of the problem is to describe adequately the quasi-1D subsystem. Let us denote the binding energies for the positions in the interstitial channels, primary chain, secondary chains, and 2D subsystem by ε_{IC} , ε_0 , ε_1 , and ε_{2D} , respectively. All of them are negative (attraction) and satisfy the following inequalities: $\varepsilon_{\text{IC}} < \varepsilon_0 < \varepsilon_1 < \varepsilon_{2D}$. As the coverage increases the particle adsorption on the nanobundle follows the order: first, the interstitial positions are occupied, then the one-chain phase is formed at the bottoms of the grooves, then it transforms to the three-chain structure and, at last, the occupation of the 2D positions occurs up to the formation of the first monolayer on the outer surface of the bundle, and so on. To simplify the model we treat the 2D adsorbate as an ideal lattice gas.

The Hamiltonian of the groove subsystem has the form

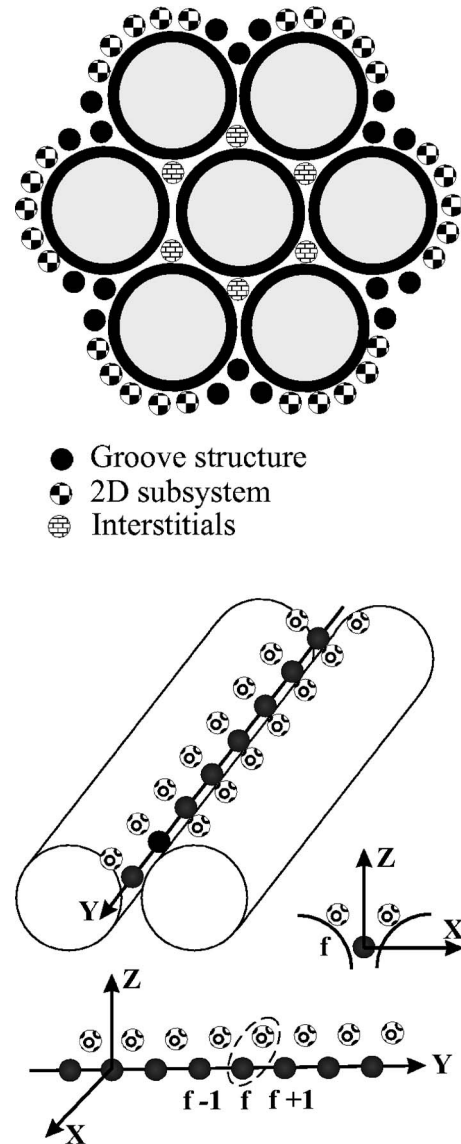


FIG. 1. The system configuration.

$$\mathcal{H} = H - \mu \sum_{f=1}^B (n_f + A_f + B_f), \quad (1)$$

$$H = \varepsilon_0 \sum_{f=1}^B n_f + \varepsilon_1 \sum_{f=1}^B n_f n_{f+1} (A_f + B_f) + H_{\text{int}}, \quad (2)$$

where n_f , A_f , and B_f are the occupation numbers of the positions in the primary and two secondary chains, respectively, which take values of 0 or 1, μ is the chemical potential, B is the total number of positions at the bottom of the groove (Fig. 1). Accordingly, the total number of positions in two secondary chains equals $2B$. The adsorption in the f th sites of the secondary chains is possible only if both neighboring sites, f and $f+1$, in the primary chain are occupied. Further,

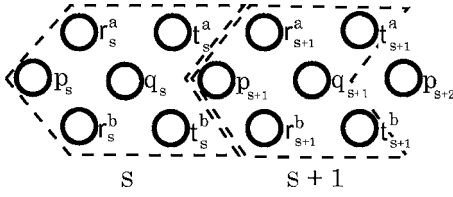


FIG. 2. Cells for the transfer-matrix method.

$$\begin{aligned}
H_{\text{int}} = & U_1 \sum_{f=1}^B n_f n_{f+1} + U_2 \sum_{f=1}^B n_f n_{f+2} + W_0 \sum_{f=1}^B n_f n_{f+1} A_f B_f \\
& + V_1 \sum_{f=1}^B n_f n_{f+1} n_{f+2} (A_f A_{f+1} + B_f B_{f+1}) \\
& + W_1 \sum_{f=1}^B n_f n_{f+1} n_{f+2} (A_f B_{f+1} + B_f A_{f+1}) \\
& + V_2 \sum_{f=1}^B n_f n_{f+1} n_{f+2} n_{f+3} (A_f A_{f+2} + B_f B_{f+2}) \\
& + W_2 \sum_{f=1}^B n_f n_{f+1} n_{f+2} n_{f+3} (A_f B_{f+2} + B_f A_{f+2}), \quad (3)
\end{aligned}$$

where U_i and V_i describe the interaction between the nearest ($i=1$) and next-nearest ($i=2$) neighbors in the primary and secondary chains, respectively, W_i is the interaction between atoms in sites f and $f+i$ ($i=0, 1, 2$) from different secondary chains.

III. TRANSFER MATRIX

To calculate the partition function of the three-chain subsystem we employ the transfer-matrix method. The system is divided into $B/2$ identical six-site cells consisting of two sites from the primary chain and four sites from the secondary chains (see Fig. 2). The total energy of the system is the sum of the cell energies E_s (s is a cell number) and the energy of the interaction between the neighboring cells $E_{s,s+1}$,

$$E = \sum_s \left(\frac{E_s + E_{s+1}}{2} + E_{s,s+1} \right), \quad (4)$$

where

$$\begin{aligned}
E_s = & (\varepsilon_0 - \mu)(p_s + q_s) - \mu(r_s^a + r_s^b + t_s^a + t_s^b) \\
& + p_s q_s [U_1 + \varepsilon_1(r_s^a + r_s^b) + W_0 r_s^a r_s^b],
\end{aligned}$$

$$\begin{aligned}
E_{s,s+1} = & q_s p_{s+1} [U_1 + \varepsilon_1(t_s^a + t_s^b) + W_0 t_s^a t_s^b] + p_s q_s p_{s+1} \\
& \times [V_1(r_s^a t_s^a + r_s^b t_s^b) + W_1(r_s^a t_s^b + r_s^b t_s^a)] + q_s p_{s+1} q_{s+1} \\
& \times [V_1(r_{s+1}^a t_s^a + r_{s+1}^b t_s^b) + W_1(r_{s+1}^a t_s^b + r_{s+1}^b t_s^a)] \\
& + U_2(p_s p_{s+1} + q_s q_{s+1}) + p_s q_s p_{s+1} q_{s+1} [V_2(r_s^a r_{s+1}^a \\
& + r_s^b r_{s+1}^b) + W_2(r_s^a r_{s+1}^b + r_s^b r_{s+1}^a)].
\end{aligned}$$

Here $p_s, q_s, r_s^a, r_s^b, t_s^a, t_s^b$ are variables taking the values of 0 or

1. They have a meaning of occupation numbers for the positions within a cell (the notations are clear from Fig. 2). Their values determine a possible configuration (state) of the s th cell. A set of all possible configurations of the s th cell forms a space of states $\sigma_s = \{p_s, q_s, r_s^a, r_s^b, t_s^a, t_s^b\}$, the total number of which is equal to $2^6 = 64$.

Finally, the transfer-matrix $\hat{T}(\sigma_s, \sigma_{s+1})$ has the form

$$\begin{aligned}
\hat{T}(\sigma_s, \sigma_{s+1}) = & \exp \left\{ -\frac{1}{T} \left[\frac{E_s(\sigma_s) + E_{s+1}(\sigma_{s+1})}{2} \right. \right. \\
& \left. \left. + E_{s,s+1}(\sigma_s, \sigma_{s+1}) \right] \right\}. \quad (5)
\end{aligned}$$

The grand partition function of the system can be represented as the product of matrices³⁵

$$\begin{aligned}
Z = & \text{tr}[\hat{T}(\sigma_1, \sigma_2) \hat{T}(\sigma_2, \sigma_3) \cdots \hat{T}(\sigma_s, \sigma_{s+1}) \cdots \hat{T}(\sigma_{B/2-1}, \sigma_{B/2}) \\
& \times \hat{T}(\sigma_{B/2}, \sigma_1)]
\end{aligned}$$

(the system is supposed to be closed into a ring and the cell number $B/2$ is adjacent to the first one). In order to calculate the partition function we need only the maximal eigenvalue $\lambda_{\text{max}}(T, \mu)$ of the matrix (5). It can be found using a well-known iterative algorithm.³⁶ As a result, the thermodynamic potential of the groove subsystem has the form

$$\Omega_{\text{GS}}(T, \mu) = -\frac{T B}{2} \ln \lambda_{\text{max}}(T, \mu). \quad (6)$$

Now all the thermodynamic characteristics of the system are calculated within the standard scheme. The conservation law for the total number of particles can be written as

$$\xi n_{\text{ads}} + (1 - \xi) n_{3\text{D}}(\mu) = n. \quad (7)$$

Here

$$n_{\text{ads}} = \zeta n_{\text{GS}} + (1 - 3\zeta) n_{2\text{D}}, \quad (8)$$

n is the particle density in the system (quasi-1D+2D+3D), ξ is the fraction of the low-dimensional positions in the system, 3ζ is the fraction of the three-chain positions in the low-dimensional subsystem, $\zeta = B/(3B + B_{2\text{D}})$, and $B_{2\text{D}}$ is the total number of the 2D positions. In addition

$$n_{\text{GS}}(T, \mu) = -\frac{1}{B} \frac{\partial \Omega_{\text{GS}}}{\partial \mu}, \quad 0 \leq n_{\text{GS}} \leq 3 \quad (9)$$

is the average number of particles in a cell of the three-chain subsystem. Further,

$$n_{2\text{D}}(T, \mu) = f_F(\varepsilon_{2\text{D}} - \mu), \quad n_{3\text{D}}(T, \mu) = f_F(-\mu),$$

$$0 \leq n_{2\text{D}, 3\text{D}} \leq 1 \quad (10)$$

are the average numbers of particles³⁴ in sites of the 2D and 3D subsystems, respectively, $f_F(x) = [1 + \exp(x/T)]^{-1}$. Equation (7) determines the chemical potential $\mu(T)$.

IV. THERMODYNAMIC FUNCTIONS OF ADSORBATE

The proposed model includes a detailed consideration of the interparticle interaction in the low-dimensional adsorbate

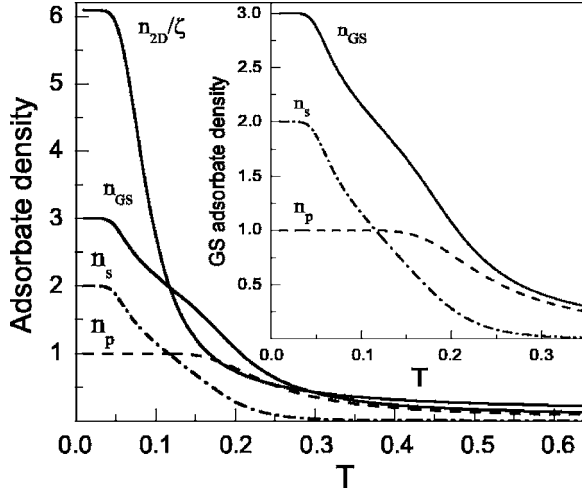


FIG. 3. Adsorbate density as a function of temperature.

and the presence of the 2D subsystem. From here on we focus our attention mainly on the features of the system behavior connected with these points.

The dependence of the thermodynamic functions on the binding energy ε_0 in the bottom of the groove was detailed in Ref. 33, and in all calculations of the present work this parameter is assumed to be constant. We choose its absolute value as an energy unit, without changing the notations for the energy parameters introduced above. Thus, $\varepsilon_0 = -1$. Below we put $\varepsilon_1 = -0.6$ and $\varepsilon_{2D} = -0.4$ unless otherwise specified.

The quantity ζ is chosen to be $\zeta = 0.13$ that is close to the corresponding value in real systems,³ and $\xi = 0.01$. Note, that the meaning of the parameter ξ is slightly different from that in Ref. 33, where the 2D subsystem was ignored. We put the total density $n = 0.02$ to make possible filling all the low-dimensional positions. Other parameters are given in tables or in figure captions.

A. Adsorbate density

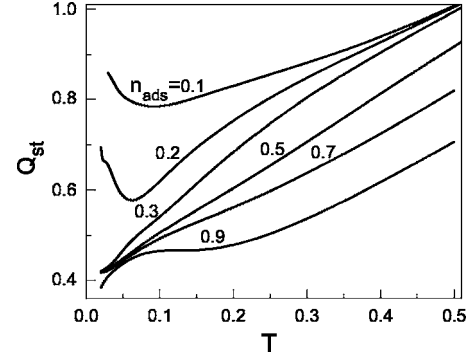
The temperature dependences of adsorbate densities $n_p(T)$ and $n_s(T)$ in primary and secondary chains, the total density $n_{GS}(T) = n_p(T) + n_s(T)$ and the density of the 2D adsorbate $n_{2D}(T)$ are shown in Fig. 3. The quantities n_p and n_s vary in the ranges $0 \leq n_p \leq 1$ and $0 \leq n_s \leq 2$. As can be seen from Fig. 3 the groove adsorbate density as a function of temperature behaves similarly to that found in Ref. 33. However, the presence of the 2D subsystem changes qualitatively the filling conditions for the 1D positions. The temperature regions where $n_p(T)$, $n_s(T)$, and $n_{GS}(T)$ are practically equal to their limiting values become narrower, because at low temperatures the groove adsorption is accompanied by an active occupation of the 2D positions.

B. Heat of adsorption

The heat of adsorption or isosteric heat is defined as⁹

$$Q_{st}(T|n_{ads}) = T^2 \left(\frac{\partial \ln P}{\partial T} \right)_{n_{ads}}, \quad (11)$$

where


 FIG. 4. Temperature dependences of Q_{st} at different n_{ads} .

$$P = \frac{T}{v_0} \ln[1 + \exp(\mu/T)] \quad (12)$$

is the pressure in the 3D lattice gas,³⁴ v_0 is the specific volume of the 3D subsystem. The derivative in Eq. (11) is calculated at fixed n_{ads} . This means that the chemical potential should be determined from Eq. (8). The balance equation (7) in this case becomes simply a definition for $n(\mu, T)$. Being the differential characteristic of the system, $Q_{st}(T|n_{ads})$ is very sensitive to the adsorbate-substrate binding energies as well as to the interparticle interactions.

Figure 4 illustrates temperature dependences of Q_{st} calculated at several values of n_{ads} . The behavior of the isosteric heat is rather different at low ($n_{ads} < 3\zeta$) and high ($n_{ads} > 3\zeta$) densities and is conditioned by redistribution of the particles among the prime chain, secondary chains, and 2D positions. The difference is more pronounced at low temperatures. If the number of adsorbate particles is less than the number of the groove positions ($n_{ads} < 3\zeta$) the function $Q_{st}(T)$ goes through a minimum and then increases as T tends to zero. At $n_{ads} < \zeta$ (the upper curve in Fig. 4) this increase in Q_{st} is caused by compaction of the adsorbate in the primary chain. Indeed, as the temperature decreases the correlation functions $\langle n_p n_{p+1} \rangle$ and $\langle n_s n_{s+2} \rangle$ tend to their minimum and maximum values, correspondingly. As a result, the desorption energy $|\varepsilon_0 + U_1 \langle n_p n_{p+1} \rangle + U_2 \langle n_s n_{s+2} \rangle|$ increases at $T \rightarrow 0$. In the region $\zeta < n_{ads} < 3\zeta$ (the curves at $n_{ads} = 0.2, 0.3$ in Fig. 4) the primary positions are completely occupied at low temperatures while the secondary chains are taken up only partially and it is the redistribution of the particles between the secondary chains that plays a dominant role and the minimum of $Q_{st}(T)$ shifts to smaller temperatures.

For dense adsorbate ($n_{ads} > 3\zeta$) the function $Q_{st}(T)$ is monotonic at $T > |U_2|$ because along with the three-chain phase completion the effect of the 2D subsystem becomes noticeable. As can be seen from Fig. 4, at high temperatures Q_{st} grows linearly with temperature. Indeed, substituting Eq. (12) in Eq. (11) and taking into account Eq. (10), we obtain

$$Q_{st} = T + T^2 \left(\frac{\partial \ln n_{3D}}{\partial T} \right)_{n_{ads}},$$

where the second term is constant at $T \rightarrow \infty$.

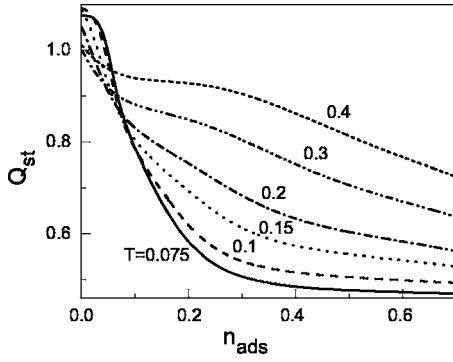


FIG. 5. Heat of adsorption as a function of adsorbate density at different T .

Figure 5 displays the theoretical curves $Q_{st}(n_{ads})$ at different temperatures. At $n_{ads} \rightarrow 0$ the isosteric heat $Q_{st}(n_{ads})$ tends to a finite limiting value $Q_0(T)$. For all the temperatures $Q_0 \geq |\epsilon_0|$ due to the contribution from the interparticle interaction. It is customary to present experimentally obtained isosteric heat as a temperature averaged function.³ As can be seen below (Sec. VI), such averaging leads to quite accurate results. However, the set of curves $Q_{st}(n_{ads})$ at different temperatures can give additional information on subtle details of the interparticle interaction.

Figure 6 demonstrates how the interparticle interaction affects $Q_{st}(n_{ads})$ at fixed temperature $T=0.1$. Curve 1 represents Q_{st} when all interactions in the Hamiltonian (3) are nonzero with near neighbor (NN) repulsion and next-nearest neighbor (NNN) attraction between atoms both in chains and between atoms from different secondary chains (see Table I). Other three curves are obtained for the case when only the NN interactions are taken into account. Curve 2 shows that neglect of the NNN attractions decreases Q_{st} at all n_{ads} . An increase in the NN repulsions leads to the sharp decrease of the isosteric heat at low adsorbate densities (curve 3), because the strong repulsion favors the particle delocalization in the grooves. Finally, if the NN repulsion between secondary chains changes for attraction (this might be the case for some bundle configurations) the isosteric heat increases at dense coverages (curve 4), where the exchange between the adsorbate and 3D atmosphere occurs mainly due to atoms from the secondary chains.

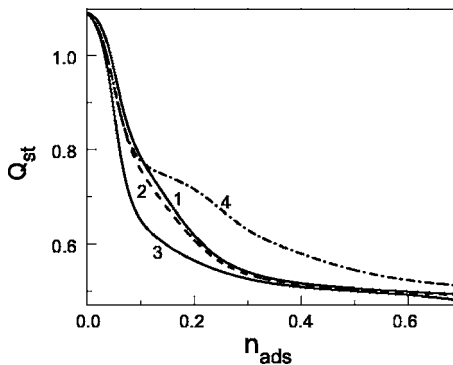


FIG. 6. Heat of adsorption as a function of the adsorbate density at different combinations of the parameters.

TABLE I. Parameters for the curves in Figs. 6 and 9.

Curve	1	2	3	4
U_1	0.1	0.1	0.2	0.1
U_2	-0.025	0	0	0
V_1	0.1	0.1	0.2	0.1
V_2	-0.015	0	0	0
W_0	0.1	0.1	0.2	-0.1
W_1	-0.02	0	0	0
W_2	-0.005	0	0	0

Figure 7 demonstrates $Q_{st}(n_{ads})$ at $T=0.1$ and different values of the binding energy ϵ_1 in the positions of the secondary chains. The behavior of the curves in Fig. 7 is quite obvious: the heat of adsorption increases with $|\epsilon_1|$.

C. Heat capacity

The energy of the system E has the form

$$E = E_{GS} + E_{2D}.$$

Here E_{GS} and E_{2D} are the energies of the groove and 2D subsystems, correspondingly,

$$E_{GS} = \langle H \rangle, \quad E_{2D} = \mathcal{B}_{2D} \epsilon_{2D} n_{2D}(T, \mu).$$

The heat capacity of the adsorbate (per site of the low-dimensional subsystem) takes the form

$$C_{ads} = \frac{\zeta}{B} \frac{\partial E}{\partial T} = C_{GS} + (1 - 3\zeta) \epsilon_{2D} \frac{\partial n_{2D}(T, \mu)}{\partial T}, \quad (13)$$

where the heat capacity C_{GS} of the groove subsystem is

$$C_{GS} = \frac{\zeta}{B} \frac{\partial E_{GS}}{\partial T}. \quad (14)$$

Temperature dependences of C_{GS} at different ϵ_1 are shown in Fig. 8. All the curves have two peaks: the high temperature peak is associated with the primary chain formation and the low temperature one is connected with the particle adsorption into the secondary chains. As $|\epsilon_1|$ increases, both peaks shift to higher temperatures. The theoretical de-

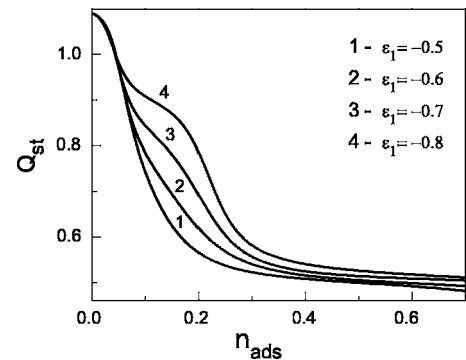
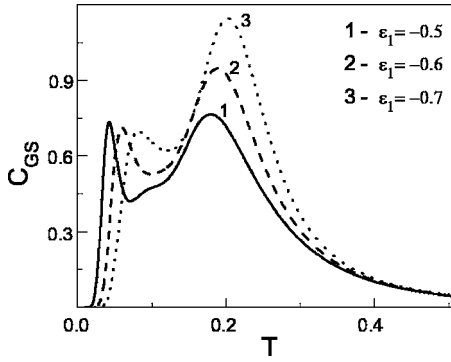


FIG. 7. Heat of adsorption as a function of the adsorbate density at different ϵ_1 .


 FIG. 8. Temperature dependences of C_{GS} at different ϵ_1 .

pendences $C_{GS}(T)$ are in qualitative agreement with the results of computer Monte Carlo simulations²⁸ on argon adsorption into the grooves.

Figure 9 shows $C_{GS}(n_{ads})$ at the same combinations of the interaction parameters as in Fig. 6 (see Table I). When the repulsions between the nearest neighbors in the chains increase both peaks of $C_{GS}(n_{ads})$ become more pronounced. At very strong repulsion the deposition into the secondary chains becomes less preferential than in the 2D positions and the second peak vanishes (curve 3).

Figure 10 shows the total heat capacity C_{ads} of the adsorbate as a function of temperature [Fig. 10(a)] and as a function of adsorbate density [Fig. 10(b)]. For comparison, the heat capacity of the groove subsystem is added to these figures. It is seen that C_{ads} does not have the two-peak shape typical of the groove subsystem due to the contribution from the 2D subsystem.

V. INTERSTITIAL ADSORPTION

The role of interstitials in the adsorption on nanobundles still remains a subject of discussion.^{1,4,23,29} It needs further experimental and theoretical investigations. At present the filling mechanism of interstitial channels is not quite understood. Indeed, an adsorbate atom should not only hit the small open face of the channel but also move forward inside the channel to vacate the place for deposition of next atoms. Thus, the mobility of the adsorbate atoms is an essential

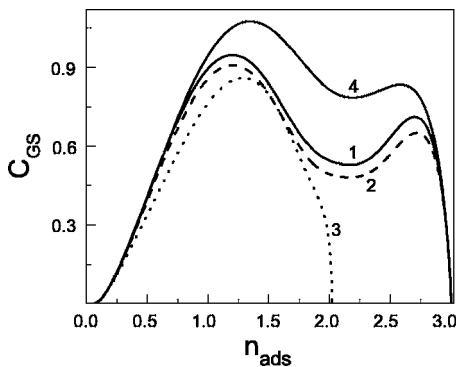
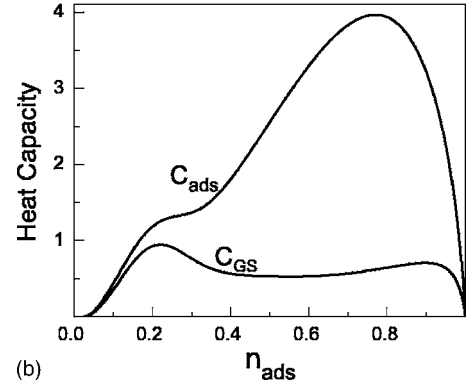
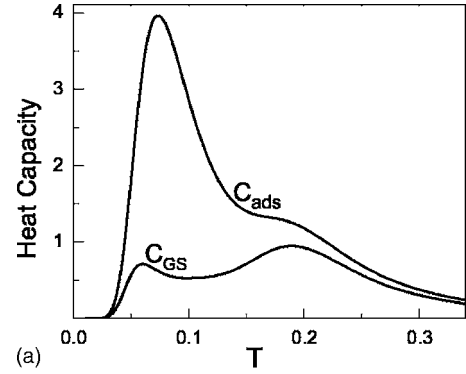


FIG. 9. Heat capacity of the GS as a function of the adsorbate density at different combinations of the parameters.


 FIG. 10. Heat capacities of the groove subsystem and the total adsorbate as functions of T (a) and n_{ads} (b).

factor controlling the interstitial adsorption. However, this problem is beyond the scope of the present paper.

Since $|\epsilon_{IC}|$ is the largest energy parameter, the contribution from the interstitials to the thermodynamics of the adsorbate is sufficient at small coverages and can be neglected at dense coverages. Experimentally,^{3,33} the effects caused by the interstitial adsorption were actually observed at $n_{ads} \ll 1$. Here we propose a simple model that gives a reasonable estimation for the contribution from the interstitials to the low-dimensional adsorption. Formally, the inclusion of interstitial positions for adsorption means the expansion of the quasi-1D subsystem. We denote by η the fraction of the interstitial positions in the total number of the quasi-1D positions. Below we assume that $\eta \ll 1$.

Let M be the number of the interstitial channels in the bundle. Each channel consists of \tilde{B} sites available for adsorption. Thus,

$$\eta = \frac{M\tilde{B}}{M\tilde{B} + 3B}.$$

The adsorbate in a channel is described within a 1D ideal lattice gas model. Due to the difference in the diameters of the nanotubes that make up the bundle the interstitial channels differ in geometry and, consequently, in binding energies $\epsilon_{IC}^{(m)}$ ($1 < m < M$). Taking into account Eq. (1), the Hamiltonian of the quasi-1D subsystem can be written as

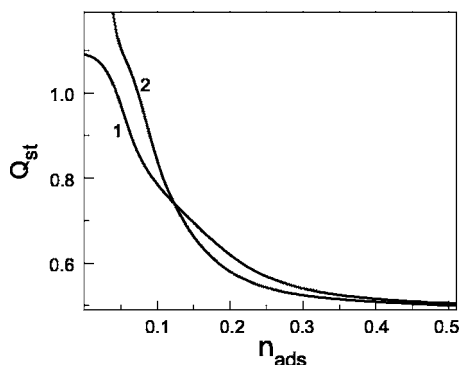


FIG. 11. Heat of adsorption with (2) and without (1) regard to the interstitials.

$$\tilde{\mathcal{H}} = \mathcal{H} + \sum_{m=1}^M (\varepsilon_{\text{IC}}^{(m)} - \mu) \sum_{f=1}^{\bar{B}} n_f^{(m)}.$$

In real nanobundles the tube diameters are distributed near some average value.³⁷ As a result, the intertube subsystem may be considered as some groups of identical channels inflated with the ideal lattice gas. In this case the average particle density on the site of the channel subsystem is given by

$$n_{\text{IC}}(\mu, T) = \sum_{\alpha} \phi_{\alpha} f_{\alpha}(\varepsilon_{\text{IC}}^{(\alpha)} - \mu), \quad \sum_{\alpha} \phi_{\alpha} = 1, \quad (15)$$

where α is the channel group number, $\varepsilon_{\text{IC}}^{(\alpha)}$ is the binding energy of the α th group, and ϕ_{α} defines the fraction of the α th group positions in the total amount of the interstitial positions.

As before, the chemical potential should be found from Eq. (7) with

$$n_{\text{ads}} = \zeta[(1 - \eta)n_{\text{1D}}(\mu, T) + 3\eta n_{\text{1C}}(\mu, T)] + (1 - 3\zeta)n_{\text{2D}}(\mu, T). \quad (16)$$

The rest of the calculations are similar to those in Sec. IV.

Figure 11 illustrates the effect of the interstitial adsorption on $Q_{\text{st}}(n_{\text{ads}})$ of the adsorbate (curve 2). For comparison, $Q_{\text{st}}(n_{\text{ads}})$ without regard to the interstitial adsorption ($\eta=0$) is also shown (curve 1). The parameters of the interparticle interaction are chosen as for curve 1 in Fig. 6, and the parameters of the intertube subsystem are given in Table II, $\eta=0.1$, $T=1$.

It is seen, that even 10% of the interstitial positions in the quasi-1D subsystem affect sufficiently the behavior of $Q_{\text{st}}(n_{\text{ads}})$ at small n_{ads} . Disregard to the interstitials leads to a plateau on $Q_{\text{st}}(n_{\text{ads}})$, which appears because at $n_{\text{ads}} \ll 1$ all the particles adsorb into the primary groove positions of equal

TABLE II. Parameters of the interstitials

α	1	2	3	4
$\varepsilon_{\text{IC}}^{(\alpha)}$	-2.0	-1.8	-1.6	-1.4
ϕ_{α}	0.1	0.2	0.3	0.4

energy. The isosteric heat of adsorption coincides with the highest binding energy of the particles with the substrate in the limit $T \rightarrow 0$ and $n_{\text{ads}} \rightarrow 0$. So, the behavior of $Q_{\text{st}}(n_{\text{ads}})$ at low coverages implies the presence of the interstitials. In addition, when we put $\eta=0$ in Eq. (16) the number of the groove positions effectively increases. As a result, there appear a difference between the curves 1 and 2 in the intermediate coverage region, where all the interstitial positions, if any, are completely occupied. Certainly, the character of the $Q_{\text{st}}(n_{\text{ads}})$ behavior in its turn is determined by $\varepsilon_{\text{IC}}^{(\alpha)}$ and ϕ_{α} .

VI. COMPARISON WITH EXPERIMENT

For today there is a detailed experimental material relative to adsorption of helium on nanobundles (see, e.g., Refs. 1 and 3). In this section we compare the obtained theoretical results with the experimental data^{3,33} on adsorption isotherms and Q_{st} for helium adsorbate. The present theory gives a quantitative description up to the coverages corresponding to the initial promotion stage of the 2D subsystem described as an ideal lattice gas. For this reason we consider only densities less than $V_{\text{ads}}=1 \text{ cm}^3$ at STP (V_{ads} is the total amount of ^4He adsorbed on the nanobundle substrate) and, therefore, the isotherms with $T > 6 \text{ K}$.

To compare the theory and experiment we should specify the parameters of the system. We begin with ζ , ξ , and η defining the geometry of the system. The value of ζ is known with a high accuracy from the structural data ($\zeta=0.13$). This is not the case for ξ because it is difficult to estimate in practice both the free volume of the experimental cell and the size of the nanobundle surface available for adsorption. However, the calculated results are not very sensitive to the value of ξ . The only important point is that at any given ξ the average density n must be large enough to make possible filling of all the low-dimensional positions. The value of η cannot be extracted from the experiment, and we choose it to provide the best agreement between the theory and experiment at low coverages, where the interstitial adsorption is important ($\eta=0.1$). To find the conversion factor between the dimensionless n_{ads} and the experimentally measured coverage density V_{ads} (in cm^3 at STP) we equate the value of V_{ads} at which the formation of the quasi-1D subsystem completes^{3,33} to the corresponding theoretical value $n_{\text{ads}}=3\zeta$.

The binding energies ε_0 , ε_1 and specific volume v_0 are chosen to fit *as a whole* the theoretically calculated set of isotherms to the set of $V_{\text{ads}}(P)$ measured experimentally. It is these parameters that are responsible for the positional relationship of the isotherms in the set.

Other parameters exert on more delicate features of the adsorption isotherms. Each of them accounts for its own coverage region. Thus, at large coverages where the contribution from the 2D subsystem prevails the correct run of the isotherms is provided for the correct choice of ε_{2D} . In the region where the formation of the GS occurs the interparticle interactions play the most important part. And at small coverages the behavior of the system can not be explained without taking into account the interstitials and, hence, the parameters $\varepsilon_{\text{IC}}^{(\alpha)}$, ϕ_{α} are determinant.

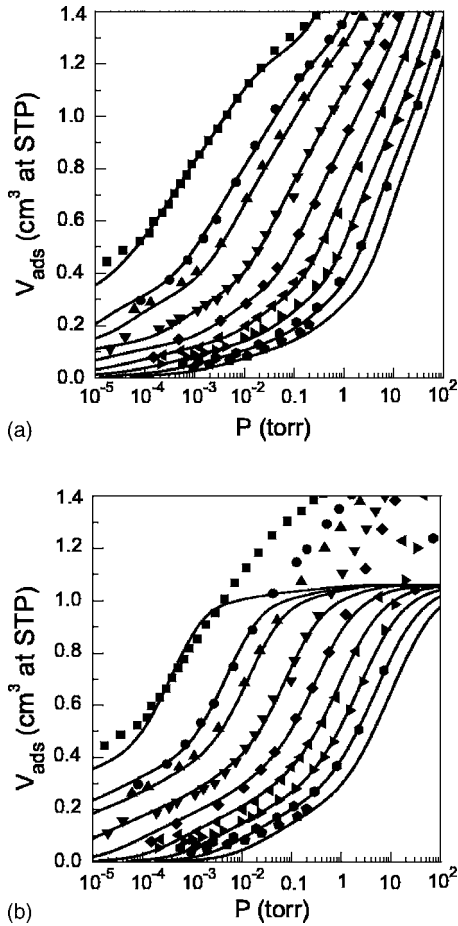


FIG. 12. The adsorption isotherms for ^4He on carbon nanobundles. Symbols are the experimental data (Refs. 3 and 33) for T (K) from top to bottom: 6.5, 7.5, 8, 9, 10, 11, 12, 13, 14. Solid curves are the theoretical results: present (a), and previous (b) (Ref. 33).

The theoretically calculated isotherms of ^4He in the temperature region 6–14 K together with the corresponding experimental data³³ are shown in Fig. 12(a). The adjustable parameters for the outer surface adsorption are the following: $\varepsilon_0 = -158$ K, $\varepsilon_1 = -115$ K, $\varepsilon_{2D} = -61$ K, $U_1 = 12$ K, $U_2 = -4$ K, $V_1 = 5$ K, $W_0 = 5$ K, $V_2 = -3$ K, $W_1 = -1$ K, $W_2 = 0$ K; and for the interstitial adsorption are presented in Table III. The obtained value of ε_0 is consistent with that found both experimentally,^{2,5} and by computer simulations.^{21,23,24} The energies of the interstitials are also in agreement with the values known from literature.^{21,23,24}

It worth noting that good agreement between the theory and experiment can be achieved only at the unique set of the parameters. For example, if we change the value of ε_0 by ± 2 K ($\sim 1\%$) the theoretical and experimental isotherms will

TABLE III. Parameters for the interstitial adsorption.

α	1	2	3	4
$\varepsilon_{\text{IC}}^{(\alpha)}$ (K)	-270	-250	-230	-210
ϕ_α	0.1	0.2	0.3	0.4

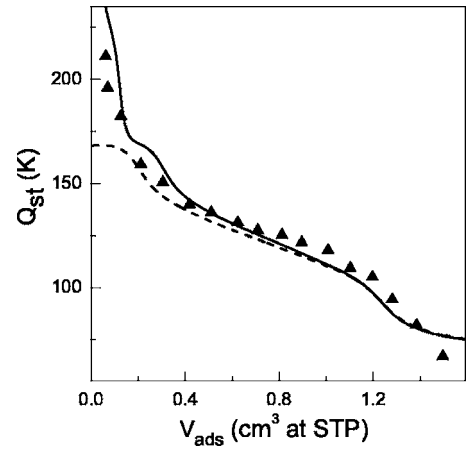


FIG. 13. Averaged heat of adsorption for ^4He on carbon nanobundles. Symbols are the experimental data (Ref. 3). Solid and dashed curves are the theoretical results with and without regard to the interstitials.

differ from each other significantly at all pressures and temperatures.

In Fig. 12(b) we show our previous results on the adsorption isotherms³³ which were calculated without regard to the 2D subsystem, interstitials and interparticle interaction in the secondary chains and between the chains. It is seen that the present model makes it possible not only to extend the region of adequate description for the adsorption isotherms but also to achieve better agreement between the theoretical and experimental results.

The experimental and theoretical dependences $Q_{\text{st}}(V_{\text{ads}})$ are shown in Fig. 13. Both curves are the results of averaging over temperature. The solid curve is obtained with regard to the interstitial adsorption, whereas the dashed one is calculated without taking the interstitials into account ($\eta=0$). The low coverage behavior of the experimentally found heat of adsorption is a direct evidence for the presence of the interstitial adsorption (see Sec. V). The solid curve reproduces all the nonmonotonocities of the measured $Q_{\text{st}}(V_{\text{ads}})$. Owing to this fact the stages of the adsorbate formation can be identified unambiguously.

The procedure of extracting Q_{st} from experimental data consists in numerical differentiation of adsorption isotherms over temperature. As a fact, this operation gives a set of $Q_{\text{st}}(V_{\text{ads}})$ at different T , but because of rather wide temperature interval between neighboring isotherms (~ 1 K) the accuracy of the corresponding derivative calculations is intrinsically limited. In this connection the experimental results on Q_{st} are typically presented as temperature averaged dependences. Theoretically, the isosteric heat can be calculated at any T without resorting to adsorption isotherms and numerical differentiation. Figure 14 demonstrates a set of the theoretically calculated $Q_{\text{st}}(V_{\text{ads}})$ for different T and the averaged experimental heat of adsorption from Fig. 13. In the given temperature region the theoretical curves cross each other at well defined nodes. The divergences of curves in loops are rather small, and averaging over temperature gives the dependence that reproduces all the features of the experimental curve $Q_{\text{st}}(V_{\text{ads}})$ quite well. Nevertheless, a lot of additional

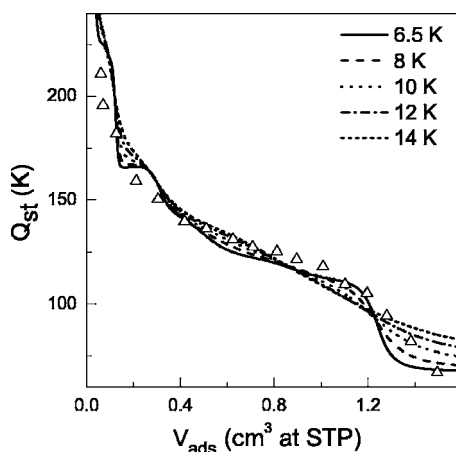


FIG. 14. Heat of adsorption for ^4He on carbon nanobundles. Symbols are the experimental data (Ref. 3). Curves are the theoretical results for different temperatures.

information about the interparticle interaction in the adsorbate can be extracted from the nonaveraged set. Thus, it is worthwhile to present experimental results for $Q_{st}(V_{ads})$ at different T .

The theory was also applied to interpret the experimental data² on methane adsorption isotherms. It turned out that a simpler model proposed in Ref. 33 is quite enough to describe adequately these data. It is due to the fact that the measurements² were carried out within the temperature range where the interparticle interactions taken into account in this work can be neglected. Moreover, the experiment was made for low coverages at which the deposition into the three-chain subsystem prevails and the formation of the 2D subsystem practically does not occur. And, finally, the filling of the interstitials is impossible due to the large size of methane molecules. As a result, the adsorption process is governed only by the attraction of the adsorbate to the quasi-1D substrate positions.

VII. SUMMARY

The analytical model has been proposed to describe quantitatively the thermodynamics of an atomic deposit adsorbed

in grooves, on the outer surface, and in interstitials of a closed-end carbon nanobundle. The model takes into account interparticle interactions between the nearest and next-nearest neighbors in the quasi-one-dimensional groove subsystem. The obtained theoretical results allow us to explain successfully the experimentally observed thermodynamic behavior of the adsorbate in the wide temperature and pressure range.

The dependences of the thermodynamic functions on the interparticle interaction parameters as well as on the attraction to the substrate have been analyzed and interpreted. It has been shown that the run of the thermodynamic functions in different temperature and density regions is determined by different interaction parameters. In fact, it is possible to detect how every single interaction parameter influences the shapes of the curves describing the densities of adsorbate in the 1D and 2D subsystems, heat capacities of the 1D and 2D adsorbate, adsorption isotherms and isosteric heat. As a result, the thermodynamic of adsorption on the nanobundles can be described on a quantitative level.

Considering the energetic constants of Hamiltonian (2) and (3) as fitting parameters, we obtain good agreement between the theory and experiment not only in general but also in all features of the experimental dependences, and this fact demonstrates the efficiency of the proposed theoretical model. We emphasize that the agreement is achieved at the unique choice of the whole set of the parameters with strongly established relationships between them. Since all the fitting parameters have clear physical meanings, it is reasonable to expect that the proposed approach can serve as a method of the “thermodynamic spectroscopy” making possible to extract the magnitudes of the interparticle interaction parameters in adsorbate directly from the thermodynamic measurements.

ACKNOWLEDGMENTS

The authors acknowledge stimulating and useful discussions with O. E. Vilches, T. A. Wilson, L. A. Pastur, and M. I. Poltavskaya.

*Electronic address: chishko@ilt.kharkov.ua

¹T. Wilson and O. E. Vilches, *Physica B* **329-333**, 278 (2003).

²S. E. Weber, S. Talapatra, C. Journet, A. Zambano, and A. D. Migone, *Phys. Rev. B* **61**, 13150 (2000).

³T. Wilson and O. E. Vilches, *Low Temp. Phys.* **29**, 732 (2003).

⁴S. Talapatra, A. Z. Zambano, S. E. Weber, and A. D. Migone, *Phys. Rev. Lett.* **85**, 138 (2000).

⁵S. Talapatra and A. D. Migone, *Phys. Rev. B* **65**, 045416 (2002).

⁶W. Teizer, R. B. Hallock, E. Dujardin, and T. W. Ebbesen, *Phys. Rev. Lett.* **82**, 5305 (1999).

⁷A. Kuznetsova, J. T. Yates, Jr., J. Liu, and R. E. Smalley, *J. Chem. Phys.* **112**, 9590 (2000).

⁸V. Simonyan, J. K. Johnson, A. Kuznetsova, and J. T. Yates, Jr., *J.*

Chem. Phys. **114**, 4180 (2001).

⁹J. G. Dash, *Films on Solid Surfaces* (Academic Press, New York, 1975).

¹⁰J. G. Dash, *Sov. J. Low Temp. Phys.* **1**, 401 (1975).

¹¹G. A. Stewart and J. G. Dash, *J. Low Temp. Phys.* **5**, 1 (1971).

¹²M. Bretz, G. B. Huff, and J. G. Dash, *Phys. Rev. Lett.* **28**, 729 (1972).

¹³M. Bretz, J. G. Dash, D. C. Hickernell, E. O. McLean, and O. E. Vilches, *Phys. Rev. A* **8**, 1589 (1973).

¹⁴R. L. Elgin and D. L. Goodstein, *Phys. Rev. A* **9**, 2657 (1974).

¹⁵D. S. Greywall, *Phys. Rev. B* **47**, 309 (1993).

¹⁶J. T. Birmingham and P. L. Richards, *J. Low Temp. Phys.* **109**, 267 (1997).

- ¹⁷T. N. Antsygina, K. A. Chishko, and I. I. Poltavsky, *J. Low Temp. Phys.* **126**, 15 (2002).
- ¹⁸A. Šiber, *Phys. Rev. B* **66**, 205406 (2002).
- ¹⁹M. C. Gordillo, J. Boronat, and J. Casulleras, *Phys. Rev. B* **68**, 125421 (2003).
- ²⁰L. Firlje and B. Kuchta, *J. Low Temp. Phys.* **139**, 599 (2005).
- ²¹M. Aichinger, S. Kilić, E. Krotscheck, and L. Vranješ, *Phys. Rev. B* **70**, 155412 (2004).
- ²²L. Vranješ, S. Kilić, and E. Krotscheck, *J. Low Temp. Phys.*, **134**, 73 (2004).
- ²³G. Stan, M. J. Bojan, S. Curtarolo, S. M. Gatica, and M. W. Cole, *Phys. Rev. B* **62**, 2173 (2000).
- ²⁴Y. H. Khang, R. B. Hallock, and M. M. Calbi, *J. Low Temp. Phys.* **138**, 217 (2005).
- ²⁵G. Stan, V. H. Crespi, M. W. Cole, and M. Boninsegni, *J. Low Temp. Phys.* **113**, 447 (1998).
- ²⁶M. W. Cole, V. H. Crespi, G. Stan, C. Ebner, J. M. Hartman, S. Moroni, and M. Boninsegni, *Phys. Rev. Lett.* **84**, 3883 (2000).
- ²⁷M. M. Calbi, M. W. Cole, S. M. Gatica, M. J. Bojan, and G. Stan, *Rev. Mod. Phys.* **73**, 857 (2001).
- ²⁸N. M. Urban, S. M. Gatica, M. W. Cole, and J. L. Riccardo, *Phys. Rev. B* **71**, 245410 (2005).
- ²⁹W. Shi and J. K. Johnson, *Phys. Rev. Lett.* **91**, 015504 (2003).
- ³⁰A. Šiber, *Phys. Rev. B* **67**, 165426 (2003).
- ³¹A. Šiber and H. Buljan, *Phys. Rev. B* **66**, 075415 (2002).
- ³²A. Šiber, *Phys. Rev. B* **66**, 235414 (2002).
- ³³T. N. Antsygina, K. A. Chishko, I. I. Poltavsky, T. A. Wilson, and O. E. Vilches, *Low Temp. Phys.* **31**, 1007 (2005).
- ³⁴T. Hill, *Statistical Mechanics* (McCraw-Hill, New York, 1956).
- ³⁵R. J. Baxter, *Exactly Solved Models in Statistical Mechanics* (Academic Press, London, 1982).
- ³⁶V. N. Faddeeva, *Computational Methods in Linear Algebra* (GITTL, Moscow, 1950) [in Russian].
- ³⁷P. J. F. Harris, *Carbon Nanotubes and Related Structures* (Cambridge University Press, Cambridge, 1999).